Remote Sensing of Environment 232 (2019) 111295

Contents lists available at ScienceDirect

Remote Sensing of Environment

journal homepage: www.elsevier.com/locate/rse

Generating intra-year metrics of wildfire progression using multiple open-access satellite data streams

Morgan A. Crowley[a,*], Jeffrey A. Cardille[a], Joanne C. White[b], Michael A. Wulder[b]

[a] Department of Natural Resource Sciences, McGill University, 21,111 Lakeshore Road, Ste.-Anne-de-Bellevue, Québec, Canada
[b] Canadian Forest Service (Pacific Forestry Centre), Natural Resources Canada, 506 West Burnside Road, Victoria, British Columbia, Canada

ARTICLE INFO

Keywords:
Fire mapping
Disturbance
Multi-source data synthesis
British Columbia
Landsat
Sentinel-2
MODIS
Google earth engine
BULC

ABSTRACT

The 2017 fire season was one of the largest on record for British Columbia (BC), Canada, in terms of total area burned (estimated 1.2 million ha), affecting the safety and air quality of numerous communities. Moreover, fires of this number and extent alter the wood supply for harvesting, the nature of habitat for wildlife, and can affect regional and national carbon budgets. As a result, it is important to map these fires accurately and to monitor within-year fire progression in order to quantify the resulting forest-disturbance impacts fully. The Bayesian Updating of Land Cover (BULC) algorithm was used to merge burned-area classifications of individual fires from a range of remote sensing sources such as Landsat-7, Landsat-8, Sentinel-2, and MODIS (MCD64A1) burned-area dataset. Together, these provisional classifications imaged each pixel within a known fire perimeter an average of 33.8 times between April 1 and December 1. The resulting 35-week time-series stack had updated weekly burned areas for each of the 89 fires in BC in 2017. Province-wide fire progression was variable throughout the period analyzed, characterized by a steady burn phase of 41,437 ha (5% of total area burned) over a two-week period in early July, an accelerated burn phase of 149,422 ha (17%) from mid-July to early August, another steady burn phase of 218,079 ha (24%) for one month until early September, and a second accelerated burn phase of 301,931 ha (34%) over two weeks in late September with subsequent steady growth of 180,119 ha (20%) over 1.5 months until containment in late October. Herein, we demonstrate how such temporally dense fire classification stacks can be used to analyze fire progression over the course of a fire season (both retrospectively and in near-real time) providing useful metrics to characterize and compare fire events. End-of-season burned-area estimates correspond with estimates derived from the National Burned Area Composite (NBAC) product that is generated retrospectively from fire best-available mapping approaches. This rapid interpretation of information enables the analysis of suppression success and potential drivers of fires spread while facilitating analyses of carbon budget consequences as well as impacts to communities and timber supply.

1. Introduction

In 2017, British Columbia (BC), Canada, faced its most severe fire season to date in terms of total area burned. Due to the severity of the wildfires, BC was in an official State of Emergency from July 7 to September 15, the longest-running State of Emergency in the history of the province (British Columbia, 2018). Single fires such as the Plateau fire grew to be quadruple the size of the total area burned in the 2016 BC fire season and a quarter of the long-term annual mean burned area for all of Canada (BC Wildfire Service, 2017a; Natural Resources Canada, 2018a). The number, size, duration, and intensity of BC's wildfires have large-scale impacts on communities, surrounding ecosystems, industries, carbon balances, and more. Reflecting upon this extreme fire season, the BC government issued a report describing the 2017 fire season as "the new normal" for wildfire conditions and vulnerability for future fire seasons within the province (Abbott and Chapman, 2018). As part of the report, recommendations were made to increase real-time, near-term and consistent mapping approaches for monitoring the fire disturbances to aid in planning and emergency responses (Abbott and Chapman, 2018). Thus, it is vital for highly systematic and rapid large-scale disaster mapping and near-term monitoring of wildfires to better aid communities and understand fire ecology and underlying factors that contribute to their behavior in these wildfire-prone areas. This recent increase in burned area and wildfire occurrence is not unique to BC, however. Longer-term trends indicate a greater fire season length at the global (Jolly et al., 2015) and increasing fuel loads and fire activity related to a changing climate in western North America (Abatzoglou and Williams, 2016), further

* Corresponding author.
E-mail address: morgan.crowley@mail.mcgill.ca (M.A. Crowley).

https://doi.org/10.1016/j.rse.2019.111295
Received 31 October 2018; Received in revised form 25 June 2019; Accepted 1 July 2019

underscoring a need for systematic monitoring efforts in Canada (Bowman, 2018).

Several national datasets capture annual area burned information for Canada. First, each jurisdiction (i.e. province or territory) maps the final perimeters of major fires; each jurisdictions' dataset is then combined to produce the Canadian National Fire Database (CNFDB; Amiro et al., 2001; Burton et al., 2009; Parisien et al., 2006; Stocks et al., 2003). A non-spatial database of burned area is also maintained by the Canadian Council of Forest Ministers (CCFM; Canadian Council of Forest Ministers, 2018). The Carbon Accounting Program for Canada's forest sector requires more detailed fire boundaries and estimates of burned area, which led to the development of the Canadian National Burned Area Composite (NBAC; Stinson et al., 2011). NBAC uses a compilation of data sources, including jurisdictional data (as per CNFDB) and satellite data such as Landsat, to capture refined fire perimeters by excluding large unburned islands and waterbodies (de Groot et al., 2007; Fraser et al., 2004). Lastly, the Composite-to-Change (C2C) protocol provides a fully automated remote-sensing-based methodology for mapping forest disturbances including burned areas, using the annual proxy best-available-pixel (BAP) composites across the 30 m Landsat record (Hermosilla et al., 2016, 2017; White et al., 2017). The cloud and gap-free BAP composites allow for similar growing conditions inter-annually, to enable long-term forest disturbance monitoring and inventorying (White et al., 2014). Each of these products provides post-hoc estimates of total national annual burned area, but there is further opportunity to map and refine near-term burned-area estimates using data from multiple Earth-observing satellites across large regions such as BC.

Several remote-sensing platforms can be used to estimate burning and burned areas at a variety of spatial resolutions for forest disturbances in Canada. The Canadian Forest Service uses data from AVHRR, MODIS, and VIIRS for its Fire Monitoring, Mapping, and Modeling (Fire M3) daily hotspot map that is publicly available and utilized by fire agencies across Canada to assess near-real-time fire activities (Fraser et al., 2000). The daily, coarser-resolution MODIS Collection 6 MCD64A1 global burned area product provides geographic locations and timing of fires at 500 m spatial resolution (Giglio et al., 2015; Humber et al., 2018). For finer scale disturbance analyses in Canadian and North American forests, spatial interpolation techniques or fusion with Landsat imagery have been used to downscale the coarse resolution of the MODIS, while at the same time leveraging the high temporal frequency of MODIS imagery and data products (de Groot et al., 2007, 2009; Hilker et al., 2009a, 2009b; Parisien et al., 2011; Parks et al., 2012; Parks, 2014). For Landsat-8 and Sentinel-2, the Normalized Burn Ratio (NBR) and its subtractive change from a pre-fire value (dNBR) provide reliable, fine-scale annual estimates of burned areas from stand-replacing fires for Canadian boreal forests (Frazier et al., 2018; Hall et al., 2008; Hermosilla et al., 2016, 2017; Key and Benson, 2006; San-Miguel et al., 2017, 2018; Schroeder et al., 2011; Soverel et al., 2010, 2011; White et al., 2017). However, the final maps created from these pixel-based burned-area mapping techniques can be heavily impacted by on-the-ground haze, smoke, and flare fire conditions that cause low-quality or missing data.

There is an opportunity for near-real-time monitoring of disturbances such as fire through data-synthesis of observations from numerous sources (Li and Roy, 2017; Wulder et al., 2018). Within-year fire progression can be constructed by fusing observations from multiple data sources into a synthesized time series, however three main limitations that remain. First, the smoke and haze from fires can obscure active fire visibility in observations from optical sources, creating difficulties for the classification of an active fire's mid-burn extent from a single-date image. Second, due to the coarse resolution of MODIS imagery, daily products detect only the largest unburned islands within fire perimeters and can result in overestimation of cumulative burned areas. Third, the processing requirements (e.g. download, correction, normalization, and interpretation) of multiple data streams over large areas for near-daily observations create a challenging image analysis environment and data processing load. Despite these challenges, there are complementary strengths of these data streams (e.g. temporal frequency of MODIS, temporal frequency and spatial resolution of Sentinel, high-accuracies for boreal forest disturbance detection of Landsat) that could potentially be combined for mapping of fires in near-real-time (e.g., Boschetti et al., 2015; Hilker et al., 2009a, 2009b; Korhonen et al., 2017; Mora et al., 2013; Roy et al., 2014; Wulder et al., 2010). Crowley et al. (2019) adapted the BULC algorithm (Cardille and Fortin, 2016; Lee et al., 2018) to map the growth and extinction of a single fire event (Elephant Hill fire) at a near-weekly frequency for a small area (< 200,000 ha). That research explored the opportunity for combining multi-source satellite image fusion for reconstructing a high-resolution burn progression time series for a single fire.

This research analyzes fire progressions for a given fire season over the entire province of British Columbia, Canada, with a forest area of approximately 60 million ha. We are able to examine the cumulative fire season trends as well as individual fire behaviors throughout the fire season. Our objectives are four-fold. First, we present a methodology for weighing multi-scale, multi-source burned-area evidence incorporating many fires over a 245-day study period using a singular, statistically-driven post-classification fusion algorithm (BULC). Second, we apply a newly available segmentation algorithm in Google Earth Engine and a multi-source dNBR technique. Third, we present an automated approach that employs the provisional classification and synthesis entirely using data and functionality made available in Google Earth Engine. Fourth, we demonstrate how the derived information outputs can be used to characterize the spatio-temporal development of the fires over the course of the fire season, introducing novel metrics enabled by the applied methods. In sum, the objective of this work is to track detailed fire progressions over an extremely large area for an entire fire season using observations from multiple sources of imagery with differing spatial, temporal, and spectral characteristics.

2. Materials and methods

2.1. Study area

The 2017 British Columbia fire season began in April, with an exceptional increase in the burned area following a series of extreme thunderstorms between July 6 to July 8, and a second surge in fire activity in August due to sustained hot and dry weather and heightened build-up of fuels (BC Wildfire Service, 2017a). The BC Wildfire Service estimated a total of 1.2 million ha burned throughout the fire season, resulting in $568 million in fire suppression costs (BC Wildfire Service, 2017a).

The four largest wildfires from the 2017 fire season comprised an estimated 80% of the total burned-area from the 2017 fire season in BC (Fig. 1). The largest fire of the season, the Plateau fire (C10784), was identified on July 7 within the Itcha Ilgachuz Provincial Park, west of Quesnel and northwest of Williams Lake (BC Wildfire Service, 2017c). This massive interface fire grew to an estimated 520,885 ha from multiple smaller fires merging (BC Wildfire Service, 2017c). The second largest fire of the 2017 fire season in terms of area burned, the Hanceville-Creek fire (C50647), was an interface fire located southwest of Williams Lake (BC Wildfire Service, 2017d). Hanceville-Creek fire was discovered on July 8 and grew to an estimated size of 239,339 ha (BC Wildfire Service, 2017d). The third fire examined, the Elephant Hill fire (K20637), was an interface fire located near Ashcroft and was used as the prototype study area in Crowley et al. (2019). It was detected on July 6 and grew to an estimated size of 192,016 ha (BC Wildfire Service, 2017e). The fourth-largest fire, the White River fire (N21628), grew to an estimated size of 26,399 ha after its identification on July 29 northeast of Canal Flats (BC Wildfire Service, 2017f).

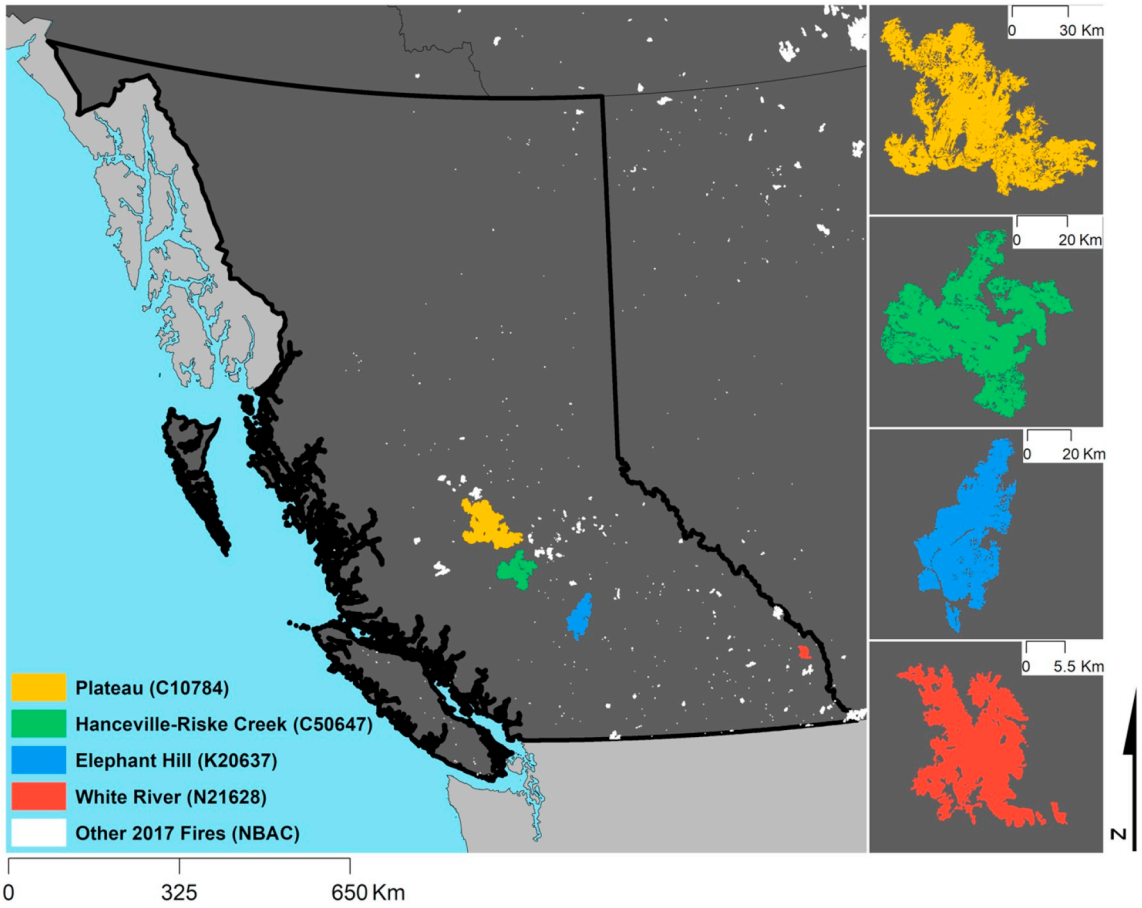

Fig. 1. The locations of the 2017 British Columbia fires, which comprise the study area, shown as NBAC polygons inside the provincial boundary. The four largest fires can be viewed individually in the panels on the right.

2.2. Google earth engine implementation

We implemented our burned-area dataset creation and analysis using a series of four stages in Google Earth Engine (Gorelick et al., 2017) shown in Fig. 2 with each stage's inputs and outputs. First, we created provisional classifications using observations from April to December 2017 within each fire's CNFDB perimeter (section 2.3). Second, we synthesized the provisional classifications together using the BULC algorithm (section 2.4). Third, we compared the end-of-season mapped fire areas to the corresponding interpretations in the NBAC dataset (section 2.5). Lastly, we produced whole-season and whole-province analyses of changing fire behaviors and patterns through time in the 2017 BC fire season. Data are described in greater detail within each subsequent methods section.

2.3. Provisional classifications using Landsat-8, Landsat-7, Sentinel-2, and MODIS

We identified 207 Landsat-8 OLI/TIRS Collection 1 Level-2 surface reflectance images, 200 Landsat-7 ETM+ Collection 1 Level-2 surface reflectance images, and 1094 Sentinel-2 MSI Level-1C images with < 20% cloud cover between April 1 and December 1, 2017, intersecting with the fire perimeters. We masked all clouds and haze before classification using the pixel-level Quality Assurance (QA) band for Landsat and Sentinel-based imagery (Egorov et al., 2018; USGS, 2018; Zhu, 2017).

We implemented the differenced Normalized Burn Ratio (dNBR; Key and Benson, 1999, 2006) on the Landsat and Sentinel imagery to create provisional classifications of burned area for each fire in each image. First, we calculated the Normalized Burn Ratio (NBR) (Key and Benson, 1999, 2006), which captures the variation between healthy vegetation and burned areas detected in the near-infrared (NIR) and shortwave infrared (SWIR) wavelengths. The ratio is calculated per-pixel for each image by dividing the NIR minus SWIR reflectance values by the NIR plus SWIR reflectance values. Low NBR values correspond with bare and burned areas and high values correspond with vegetation.

Each active-fire NBR image was segmented into median-NBR objects using the Simple Non-Iterative Clustering (SNIC) segmentation algorithm available in Google Earth Engine (Achanta and Süsstrunk, 2017). Segmentation algorithms like SNIC create pixel clusters using imagery information such as texture, colour or pixel values, shape, and size and is especially useful for forest disturbances (Blaschke, 2010; Wulder et al., 2004). Many fire-detection methods rely on pixel-based approaches, but image segmentation offers advances for the refinement of burned-area imagery (Gitas et al., 2004; Veraverbeke et al., 2012). In particular, SNIC is a bottom-up, seed-based segmentation approach that

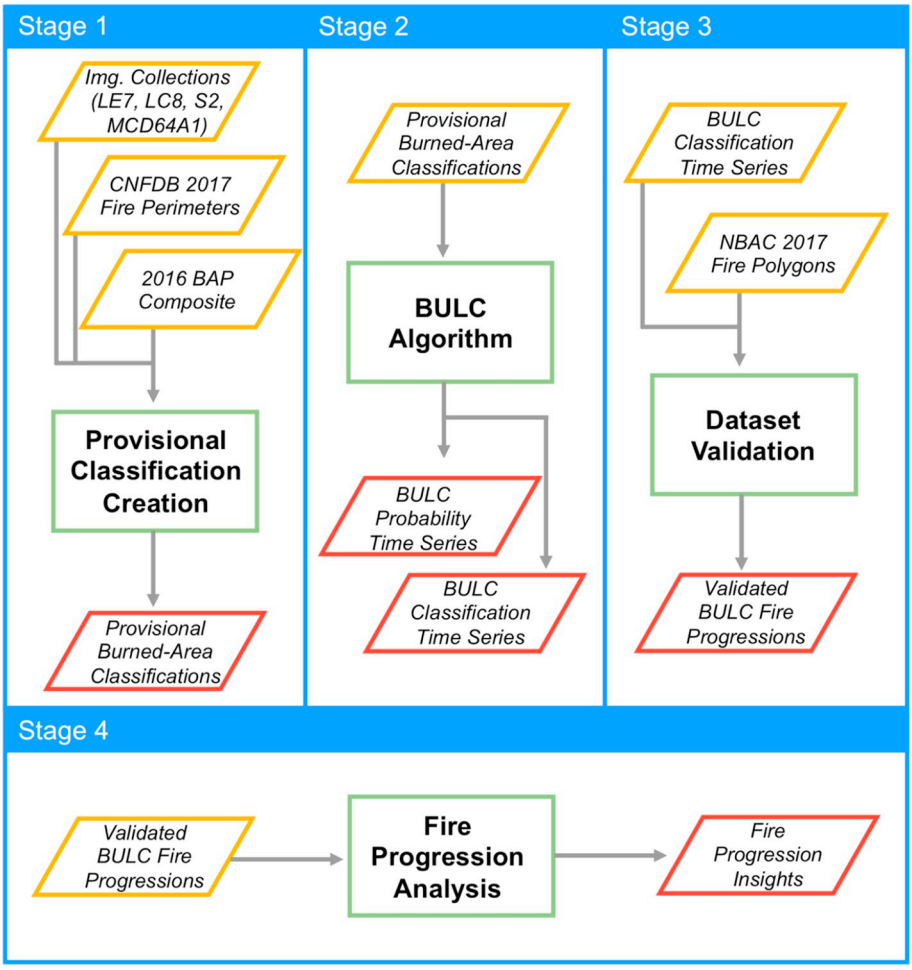

Fig. 2. Outline of the four stages of analysis for this research, shown in a simplified flow chart (yellow represents inputs, green represents processes, and red represents outputs). Stage 1 (left) created provisional classifications that were then used in the BULC algorithm in Stage 2 (center). The output from Stage 2 was used in the validation in Stage 3 (right). The validated outputs from Stage 3 were then analyzed further in Stage 4 (bottom). (For interpretation of the references to colour in this figure legend, the reader is referred to the web version of this article.)

groups neighboring pixels together into clusters based on input data and parameters such as compactness, connectivity, and neighborhood size. To segment each active-fire NBR image, we set the SNIC parameters as follows: compactness was set to 0.1 to enable larger clusters, connectivity was set to 8, the neighborhood size was set to 8 pixels to avoid tile boundary artifacts, and the seeds were created in a hexagonal pattern using a superpixel seed spacing of 4 pixels.

Using the 2016 BAP composite a pre-fire expected NBR; we calculated the differenced Normalized Burn Ratio (dNBR) using each segmented active-fire NBR image. The dNBR is calculated by subtracting the post-fire NBR from the pre-fire NBR, where negative and lower values correspond with regrowth and unburned vegetation and higher values correspond with fire severity (Key and Benson, 2006). The dNBR index is often calculated using single-source imagery, however, observations from pre-fire Landsat-8 and post-fire Sentinel-2 can be combined to enable retrospective mapping without impact on stand-replacing fire map accuracy (Quintano et al., 2018). For this reason, we utilized the 2016 BAP gap-free surface reflectance composite that was generated following the C2C approach to calculate the pre-fire NBR to compare with Landsat-7, Landsat-8, and Sentinel-2 observations (e.g., Hermosilla et al., 2016, 2017; White et al., 2014, 2017). We differenced the segmented active-fire NBR of each image with the pre-fire NBR to produce 259 dated provisional classifications from Landsat-7, -8 and Sentinel-2 for use in BULC, from 157 distinct dates during the study period. This approach pre-processed each dNBR image with temporal contextualization from the BAP protocol and spatial normalization from the segmentation. Differences over the stand-replacing fire dNBR threshold (dNBR > 0.284) for moderate to high severity, as outlined in Hall et al. (2008), were classified as 'Burned/Burning'; those below the threshold were classified as 'Unburned' at that time step (e.g., Crowley et al., 2019; Frazier et al., 2018).

To create the MODIS provisional classifications, we summarized 15-day burned areas from the MODIS Collection 6 MCD64A1 burned area product as classifications (Giglio et al., 2015; Humber et al., 2018). This raster data product detects day-of-burning globally at 500 m resolution with an average uncertainty of 5.3 days and a processing delay between

1.5 and 2.5 months for the 2017 BC fires. Each monthly MODIS burned-area raster contains the detected day-of-burn for pixels, we reclassified these MODIS burned-area products into Burned/Burning and Unburned layers in 15-day summaries. The result was 17 date-specific summary classifications that were used as inputs to BULC.

In total, we classified 276 provisional classifications spanning 167 distinct imaging dates during the study period. The 83 Landsat-8 surface reflectance classifications, 76 Landsat-7 surface reflectance classifications, 100 Sentinel-2 classifications, and 17 MODIS bi-weekly classifications were ordered by date and used as provisional classification inputs in the BULC algorithm. Combined, these sensors imaged each pixel within the fire perimeters an average of 33.8 times between April 1 and December 1, with the entire study area imaged approximately once in each of the 35 weeks of the fire season.

2.4. Bayesian updating of land cover (BULC) algorithm

We used the BULC algorithm to fuse the burned-area information from the four sources for the 2017 fires (Cardille and Fortin, 2016; Crowley et al., 2019). BULC applies Bayes' Theorem to each pixel within each time-ordered provisional classification. The provisional input classifications are used as the prior knowledge in Bayes' Theorem and contribute to the synthesized time series summarizing evidence-based change and stability for each pixel. First, provisional classifications are ordered temporally and compared pixel-by-pixel to calculate their correspondence in an agreement matrix. This agreement matrix serves as conditional probabilities in Bayes' formula, which are then tracked for each class in each pixel for the duration of the time series. BULC traces the probability of two classes, burned and unburned corresponding to the two classes from the dNBR classifications. Probabilities are updated through time using new evidence provided by each new provisional classification in the stack. The most-likely class per pixel is evaluated to create the BULC classification at each time step in the series.

BULC can be used to fuse varying-quality classifications over fine temporal scales to track rapidly changing landscapes, as detailed in the context of a 2013 wildfire in Quebec in Cardille and Fortin (2016). Like other burned-area classifying algorithms (Padilla et al., 2014, 2015), BULC's burned-area estimations correspond with the availability of images from a given provisional classification source. For example, if clear observations from a single source are only available monthly, this can cause a delay in the temporal burn date given by BULC. As BULC is sensor-independent (Cardille and Fortin, 2016), data acquired by more sensors can be considered by the algorithm to improve the frequency and accuracy of the fire sequence to rectify any temporal gaps in imagery availability from a single source. Additionally, BULC can accommodate occasional errors such as from smoke, clouds, haze by relying on the input classifications from multiple data sources to fill temporal and quality gaps in imagery.

A previous study has demonstrated the ability for BULC to fuse information from multiple data sources into a singular, consistent fire progression dataset in British Columbia for a large fire event (203,560 ha; Crowley et al., 2019). Fusing images from Sentinel-2, Landsat-8, and MODIS, BULC leveraged the temporal and spatial resolution strengths of data from each sensor to produce a spatially-explicit time series that documented the fire's changing patterns at sub-weekly time scales and at the 30 m spatial resolution of Landsat. Therefore, BULC is able to estimate the burned area of an active fire at intermediate time steps relying on a dense stack of relatively clear provisional classifications from multiple sources in Google Earth Engine.

2.5. Agency data for fire perimeters and burned-area estimates

2.5.1. Canadian National Fire Database (CNFDB)

At the end of the fire season, the BC Wildfire Service digitizes official fire perimeters for each fire available in a vectorized dataset that is then used in the CNFDB compilation of fire perimeters across Canada. For the 2017 fire season, the most commonly used methods for delineating BC fire perimeters were ground/airborne GPS, manual sketches from observers in aircraft, and remote sensing image digitization (e.g., satellite, aerial, digital camera). The 2017 fire season dataset had 379 distinct fire perimeters for BC, capturing the final extent and estimated burned area for each fire as determined by the various provincial fire agencies (BC Wildfire Service, 2017b). Of the 379 fire polygons included in the CNFDB database, there were 290 fire polygons that were either duplicate polygons or grew to be less than < 100 ha in provincially calculated burned area. As these fires typically burned for a limited period (i.e. only a few days), they were removed for consideration. This dataset provides the estimated burned area for the province each year, and these estimates are further refined following the fire season by the remote-sensing supported NBAC dataset.

2.5.2. National Burned Area Composite (NBAC)

The NBAC is created in the year following each fire season to provide a more spatially refined, vectorized burned area dataset for Canada's Carbon Accounting Program (Stinson et al., 2011). For the 89 fires from the 2017 fire season, the most commonly used method for delineating the NBAC burned area polygons was using the Canadian Forest Service/Canadian Center for Remote Sensing fine spatial resolution derived products from Single Acquisition Fire Mapping System (SAFiMS) or Multi Acquisition Fire Mapping Systems (MAFiMS) software on Landsat-based satellite imagery (Table 1). For NBAC, SAFiMS and MAFiMS satellite mapping is done manually for each fire using pre- and post-fire images, assessed in areas of the country with sufficient levels of fire activity. The final NBAC product is generated using a rule-based algorithm to select the best-available data source for each fire event, considering the quality of the data source and the methods used for mapping. For the 89 fires from the 2017 BC fire season, 57 NBAC fire events were created from SAFiMS/MAFiMS processing of Landsat imagery, including the four largest fires: Plateau, Hanceville-Riske Creek, Elephant Hill, and White River. The remaining 32 NBAC fire polygons were based on fire agency polygons (e.g., CNFDB), created either from manual sketches or ground/aerial GPS data.

Table 1
NBAC Dataset metadata for 89 2017 BC fires including data provider and fire mapping method and source.

Data provider	Fire mapping method and source	Total fires mapped
NRCan Remote Sensing	SAFiMS/MAFiMS on Landsat imagery	57
Provincial Fire Agency	Aerial survey GPS	18
	Field survey GPS	9
	Hand sketch	3
	Undefined	2

2.6. Comparison of burned-area estimates

The NBAC was used for comparison against the end-of-season BULC burned area maps to assess the degree of correspondence in burned area estimates. First, we cross-tabulated the pixels of the NBAC data and BULC at each time step. Using these cross-tabulations, we calculated the Dice Coefficient for each date and bias in terms of proportion of burned area between the NBAC data with the BULC end-of-series burned-area map, following the validation methods employed in Padilla et al. (2015). In particular, the Dice Coefficient in this scenario estimates the spatial overlap between the BULC fire-progression dataset and the NBAC dataset, ranging from 0 (no agreement) to 1 (complete agreement) (Padilla et al., 2014, 2015).

2.7. Fire progression metrics

Availing upon the unique information provided by the BULC fire progression data, we generated a number of metrics to characterize the 2017 fires in BC (Table 2). These metrics quantify the spatio-temporal characteristics of the fires in both summary and comparison values that can be used to describe and compare the fire season and individual fire behaviors. Fire metrics can be calculated at various temporal scales, including daily, weekly and entire fire season. Additionally, these metrics can be calculated relative to the fire season's calendar days/weeks to examine fire season features or relative to the individual fire's day of fire to examine fire-specific features.

3. Results

3.1. Correspondence of BULC burned area dataset for BC

We calculated the Dice Coefficient, bias, relative bias, and relative difference to quantify agreement between the NBAC and BULC dataset (Table 3). The average relative difference in burned area was −7.5% for larger fires with an average Dice Coefficient of 0.76 (e.g., Plateau, Hanceville-Riske Creek, Elephant Hill), and −16.0% for smaller fires

Table 2
Definition and purpose for each fire progression metric, where n is the burned area on a given day (d) or week (w).

Fire progression metric	Definition	Purpose
Cumulative burned area	Total burned area at each time step per fire or per fire season in hectares (n_t)	Summary metric for burned area over time
Cumulative area relative to max area	Proportion of cumulative burned area divided by maximum burned area per fire (n_t / n_{max})	Comparison metric for burned area over time
Daily burned area	Burned area growth from prior time step to current time step per fire in hectares ($n_d - n_{d-1}$)	Summary metric for daily burned area change
Daily burned area relative to max area	Proportion of daily burned area divided by maximum burned area per fire ($n_d - n_{d-1}$)/(n_{max})	Comparison metric for daily burned area changes
Number of active fires	Count of total fires actively burning at each time step	Summary metric indicating combined fire season activity
Number of fires at peak burn week	Count of fires per week that have their maximum *Weekly relative change in burned area*	Summary metric indicating fire season activity per fire
Weekly observation rate	Average number of observations per fire per week during its active phase and across entire fire season	Summary metric for data availability per fire
Weekly relative change in burned area	Proportion of burned area growth from the past week divided by previous week's burned area amount ($n_w - n_{w-1}$)/(n_{w-1})	Comparison metric for relative weekly burned area changes per week

Table 3
Dataset validation using the National Burned Area Composite (NBAC), the relative difference and the Dice coefficient was calculated using the correspondence between the BULC final dataset against individual fire polygons from the NBAC dataset.

Fire region	BULC (ha)	NBAC (ha)	Relative difference (%)	Dice coefficient
All BC fires	890,988	1,057,998	−15.79	0.73
Plateau (C10784)	381,168	410,382	−7.12	0.75
Hanceville-Riske Creek (C50647)	199,075	214,293	−7.10	0.76
Elephant Hill (K20637)	165,894	180,867	−8.27	0.76
White River (N21628)	16,164	23,153	−30.19	0.66

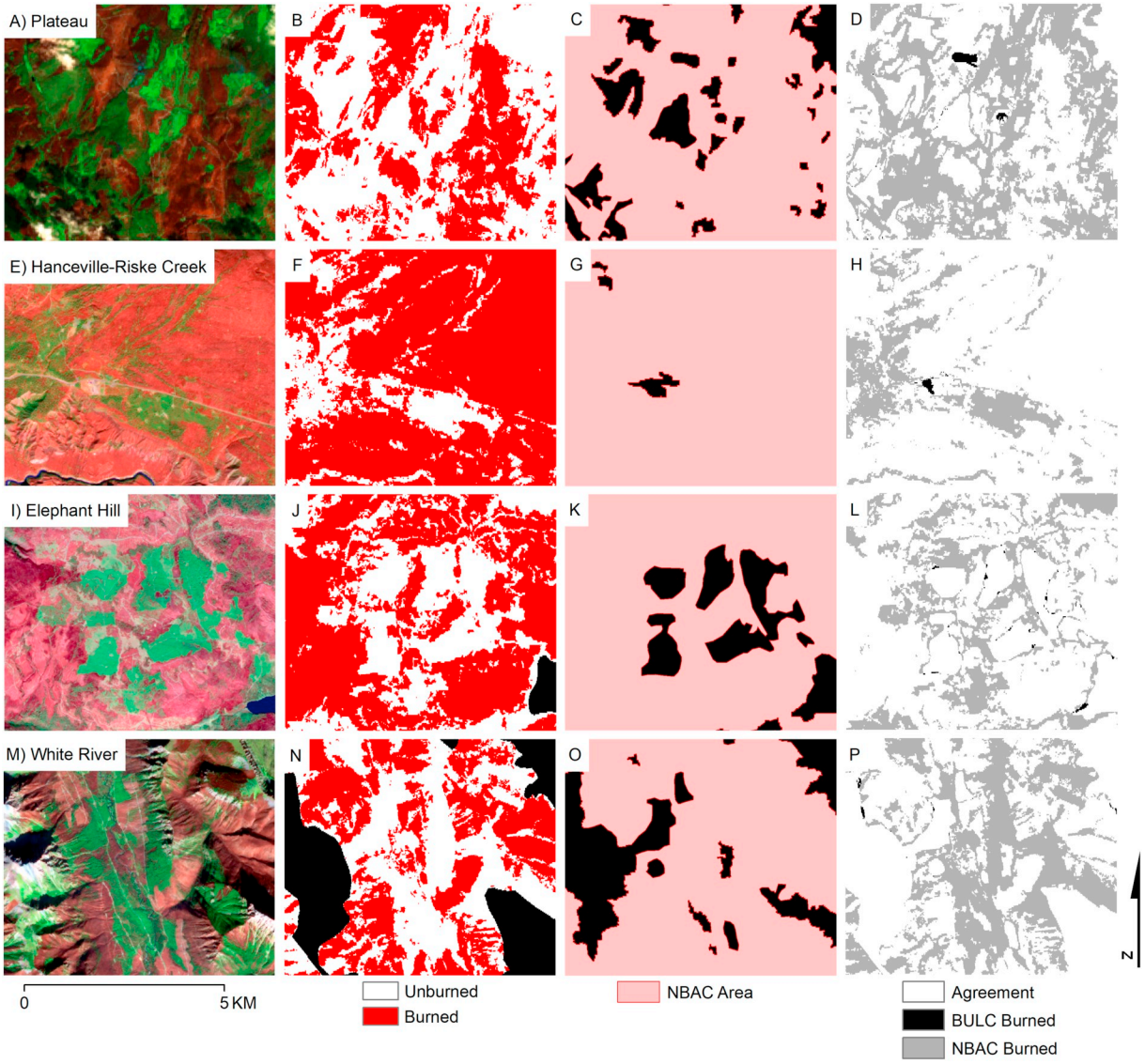

Fig. 3. For each fire (rows), zoomed final burned area Landsat-8/Sentinel-2 composite in column 1 (A, E, I, M), corresponding BULC final classification in column 2 (B, F, J, N), corresponding NBAC burned area polygon in column 3 (C, G, K, O) and fire agreement between burned area from the BULC fire progression dataset and the burned area from the NBAC dataset in column 4 (D, H, L, P). In the Landsat-8 and Sentinel-2 composites in column 1, red areas correspond with burned area. (For interpretation of the references to colour in this figure legend, the reader is referred to the web version of this article.)

that had lower average Dice Coefficient of 0.61 (e.g., White River). The bias and relative bias for all BC fires pointed towards the BULC dataset estimated the burned area as lower compared to the NBAC dataset (i.e., bias of −0.34, relative bias of −0.41). The lower estimation of burned area in the BULC-derived dataset is most evident on the edges of burned objects when comparing the BULC and NBAC datasets (Fig. 3). Both datasets have strong agreement (i.e., ~99% on average) in the clearly unburned and much of the burned area (Fig. 3D, H, L, P), and the BULC dataset tends to provide a lower estimate of burned areas corresponding with the satellite imagery. The level of correspondence between the BULC burned area estimate with the NBAC dataset builds confidence in the BULC outputs.

In Fig. 4, we compare the datasets in terms of their refined capabilities, showing the final BULC classification for Elephant Hill fire against the raw Sentinel-2 image for the fire, the polygons marking the CNFDB fire perimeter and NBAC burned area, and the final MODIS burned area dataset for this fire on October 4, 2017 (following its containment). Evident refinement has been made in burned-area detection to Landsat resolution with this BULC burned area dataset with burned-area agreement with the existing refined datasets, while also

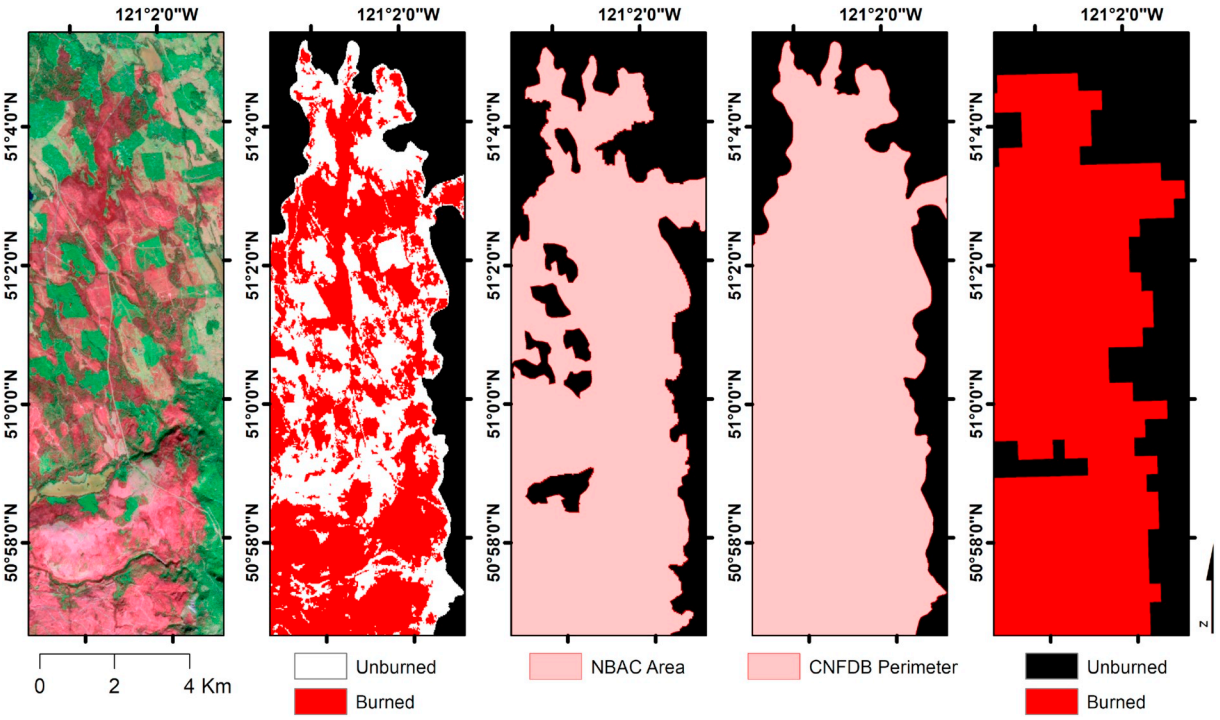

Fig. 4. Burned-area dataset comparisons against final burned area Sentinel-2 image from October 3 in (A) for the Elephant Hill fire zoomed in at fire edge at 51°10′ N, 121°2′W. The resulting October 3 BULC classification within the CNFDB fire boundary is shown in (B), highlighting the fine spatial resolution. The NBAC burned area polygon dataset is shown in (C), the CNFDB polygon perimeter dataset is shown in (D), and the final MODIS burned area is shown in (E).

creating fire progression details that will be further examined in the subsequent sections.

3.2. Fire progression metrics

BULC synthesized provisional input classifications from the fire season, which allows per-pixel burn progressions within the British Columbia fire-event perimeters at the collection date of each provisional classification. Considered together, the 89 fires of the 2017 fire season burned unevenly temporally through the summer and autumn (Fig. 5). The cumulative area burned through the fire season was irregular and was characterized by a steady burn phase of 41,437 ha for two weeks from its start in early July to mid-month, an accelerated burn phase by 149,422 ha for two weeks from mid-July to early August, a steady burn phase of 218,079 ha for one month from early August to early September, and a second accelerated burn phase of 301,931 ha for two weeks from early September to mid-September, and subsequent steady growth by 180,119 ha for 1.5 months from mid-September until containment in late October.

Provisional, burned-area classifications were synthesized together in the same time series stack by BULC, and using that dataset, individual fire progressions for each fire polygon can be examined in greater detail. The four largest fires of 2017 (Fig. 6A) accounted for 86% of the total 2017 burned area in BC. Individual fires varied in the timing of their burned area and burn rates, with many smaller fires burning quickly to their final size (Fig. 6B) while the larger fires experienced longer burn periods. Many smaller fires grow to their final burned area within a single day (Fig. 6B, C), indicating these fires were extinguished quickly and contained to a smaller area. The largest fires grew to their final burned areas more gradually (6B), but with spikes in daily burned area following a widespread lightning storm that caused many ignitions across BC (Fig. 6D).

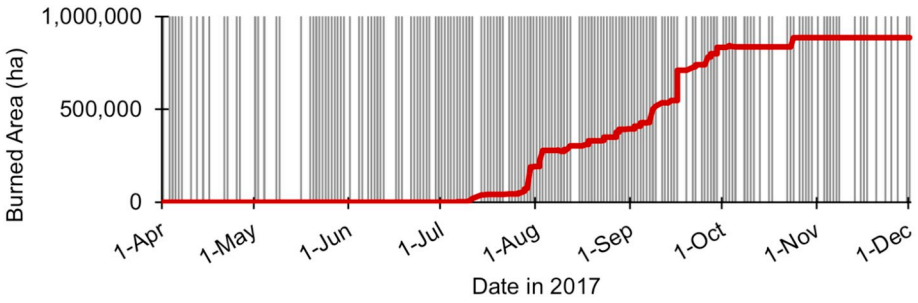

Fig. 5. Cumulative burned-area progression for the 89 fires in 2017 in British Columbia, Canada, from the beginning of the fire season in April to December 1, with provisional classification frequency denoted by grey bars.

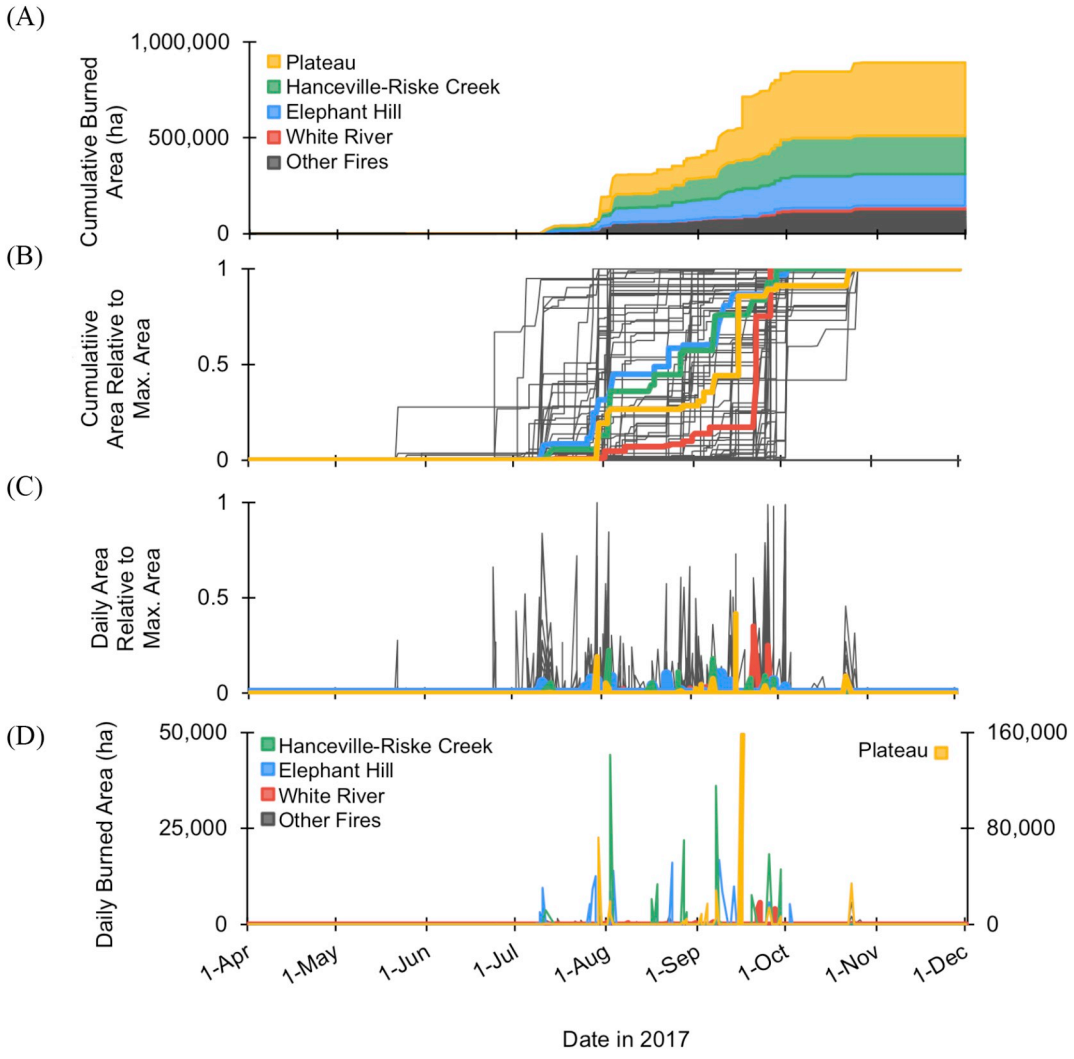

Fig. 6. Individual fire (A) cumulative burned-area progression in ha, (B) cumulative burned-area progression relative to maximum area, (C) daily burned area relative to maximum burned area, (D) daily burned area in ha for each of the 89 fires in 2017 in British Columbia, Canada, from the beginning of the fire season in April to December 1, with the four fires presented in greater depth in the following sections colored uniquely.

By examining the maximum size and burned-area growth rates of the individual fires (Fig. 6), we developed a heuristic to characterize the 2017 fires, characterizing them according to size (small versus large) and their rate of spread (slow versus fast). Large fires grew to be > 20,000 ha in total burned area, while small fires were smaller than 20,000 ha. Fast fires grew > 40% of their burned area in a single week, while slow fires did not. Of the 89 fires we analyzed, 13 were small and slow fires growing to their final extent of < 20,000 ha steadily across the fire season. These small and slow fires accounted for 3% of the total burned area of the 2017 fire season. By contrast, small and fast fires (n = 72) were < 20,000 ha in size and had rapid growth periods over their actively burning period (e.g., growing to over 40% of their burned area within a single week like the White River). Small and fast fires accounted for 13% of the cumulative burned area for the 2017 fire season. Two fires were large fires (> 20,000 ha) and had dispersed growth periods throughout their active phase (e.g., Hanceville-Riske Creek, Elephant Hill). These two large and slow fires accounted for 41% of the cumulative burned area for the fire season. One fire, the Plateau fire, was a large and fast-moving fire that had rapid growth weeks over 40% of its final burned area. This single large and fast developing fire event accounted for 43% of the cumulative burned area for the 2017 fire season.

Fire progressions and corresponding metrics can be summarized to weekly attributes to better identify key periods of the fire season. For fires of all sizes, there were two key periods of individual fire growths compared to previous weekly burned areas, occurring in week 18 (end of July) and week 26 (mid-September) of the fire season (Fig. 7A). The number of fires actively burning increased notably by 33% between July 16 and July 27, corresponding with a widespread lightning storm on July 17 that caused many ignitions across BC (Fig. 7B). 22 fires had their peak burn weeks in week 18 (July 29) following the lightning storm, and 21 additional fires had their peak burn week during week 26 beginning on September 23 (Fig. 7C). BC fire agencies employed many resources to contain all of these growing fires during their peak burn weeks in July (Fig. 7B, C; Abbott and Chapman, 2018). However, the four largest fires steadily grew out of control following that period to contribute the largest areas to the cumulative burned area and the largest daily burned areas (Figs. 6A, D, 7A). Following the second peak

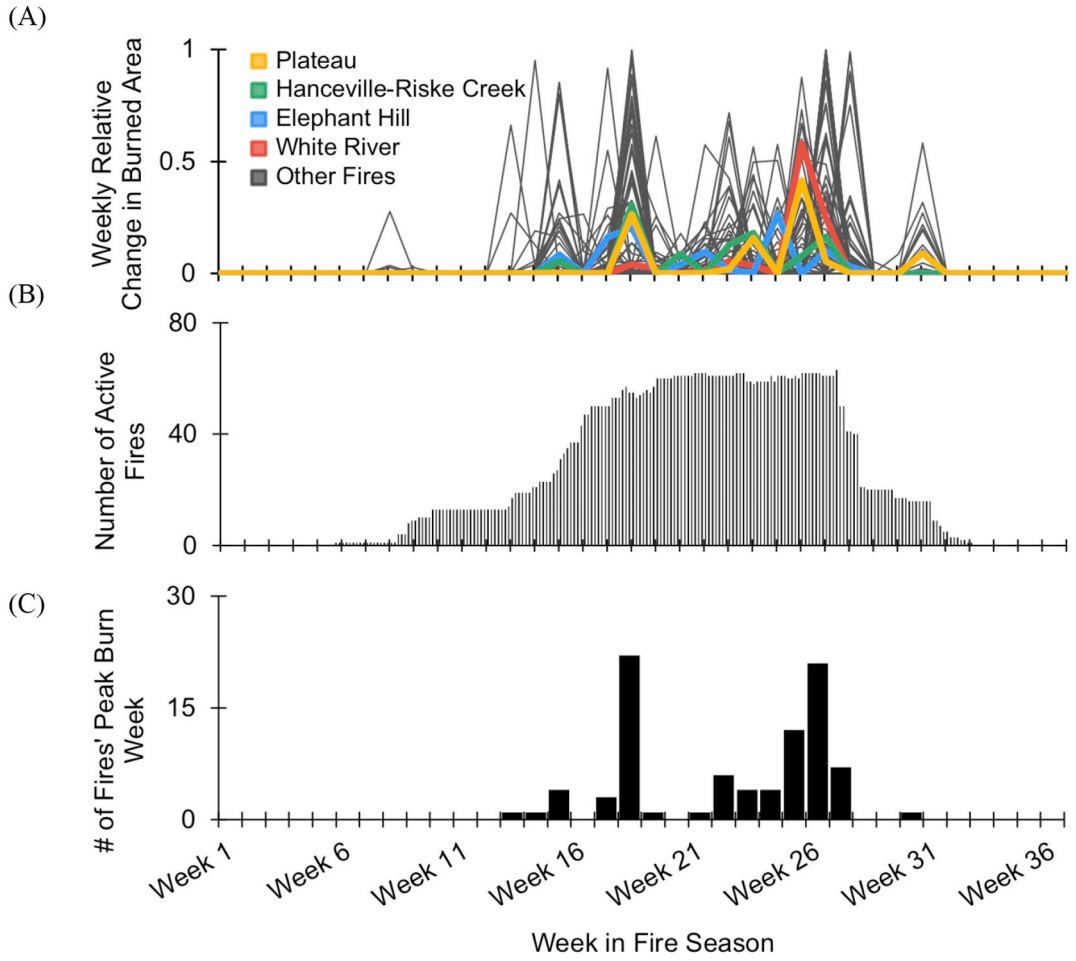

Fig. 7. Weekly fire season attributes, including (A) weekly relative change in burned area for each fire, (B) number of active fires, (C) number of fires' peak burn weeks, from the beginning of the fire season in April to December 1, with the four fires presented in greater depth in the following sections colored uniquely.

burn week in mid-September, 67% of the fires were extinguished between September 23 and October 7 as shown by the decreasing total count of active fires after week 26 (Fig. 7B).

3.3. Individual fire attributes

There were consistent observations throughout each fire's active phase that helped delineate their individual burn progressions (Fig. 8). The Plateau Fire was the largest fire from the 2017 BC fire season and was a large and fast-moving fire that grew in distinct burn phases over the duration of its long actively burning period of 10 weeks (Fig. 8a). The burn progressions for the Plateau fire for the entire fire season highlights these large increases in burned areas at the end of July and middle of September. The Hanceville-Riske Creek Fire was the second-largest fire from the 2017 BC fire season and was a large and steady growing fire over the duration of its 11-week burning period (Fig. 8B). The burn progression for the Hanceville-Riske Creek depicts steady increases in burned areas throughout the fire's active phase. The Elephant Hill fire was a large and steady 12-week burning period, with two larger increases in burned area of the fire at the end of July and during the middle of September (Fig. 8C). The fourth largest 2017 BC fire, the White River fire, was a small and fast burning fire during its 9-week burning period and had a rapid jump in size at the end of September following a steady increase in burned/burning area (Fig. 8D).

Each of these fires had distinct peak burn week that contributed to a majority of their total burned areas, and we can view the pre-peak week and post-peak week BULC classifications to better visualize the fire behaviors (Fig. 9). Prior to its peak burn week in mid-September, the Plateau fire had already burned nearly 120,000 ha (30% of total burned area) by September 2 in distinct, separate smaller fires that were joined together in its peak burn phase (Fig. 9A, B). The Hanceville-Riske Creek fire had a peak burn week in the end of July following its growth to 68,636 ha (34% of total burned area) on August 3 after its ignition in early July (Fig. 9C, D). The Elephant Hill fire grew to 66,767 ha (40% of total burned area) on August 4 after its ignition in early July and prior to its peak burn week at the end of July (Fig. 9E, F). Lastly, the White River fire had its peak burn week in mid-September after growing to 2236 ha (14% of final burned area) on September 1 (Fig. 9G, H). BULC

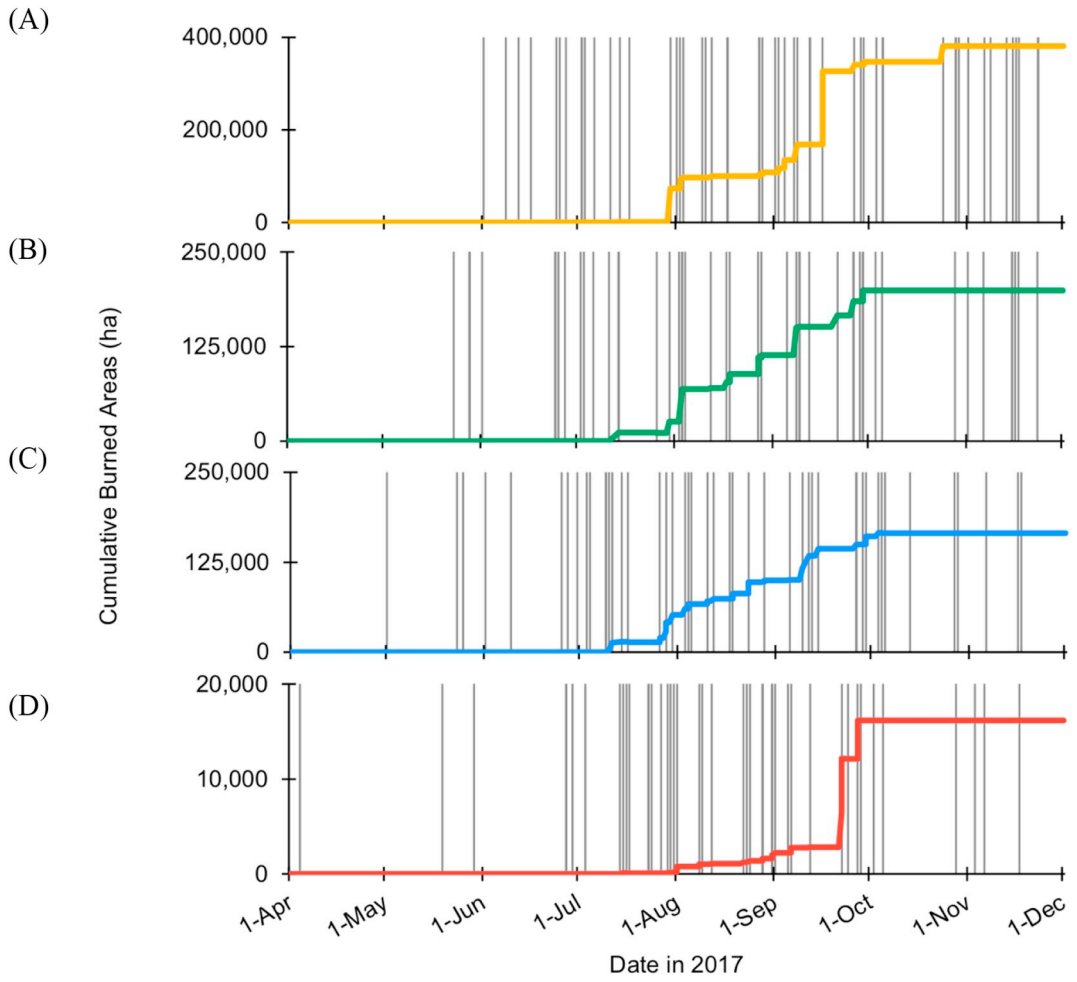

Fig. 8. Burned-area progression tables for individual fires, including (A) Plateau, (B) Hanceville-Riske Creek, (C) Elephant Hill, (D) White River, from the beginning of the fire season in April to December 1, with observation frequency denoted by grey bars. The denser the grey bars in the figure, the more observations included in BULC as provisional classifications.

classifications for distinct dates of interest can be mapped individually in addition to being summarized in date-of-burned-observation maps.

When the burn history presented by BULC can be charted for each large fire (e.g., Fig. 8), it is possible to also map the spatio-temporal dynamics of each fire as it progressed (Fig. 10). For the Plateau fire, the fire had grown to its maximum extent near October 24 at 381,168 burned ha (Fig. 10A B) from several smaller fires that grew together rapidly late in the fire season (Fig. 10C). The Hanceville-Riske Creek fire grew to its final extent by September 29 at 199,075 burned ha (Fig. 10D, E) steadily outward from its central ignition location (Fig. 10F). The similarly sized Elephant Hill fire grew to its final extent by October 3 at 165,894 burned ha (Fig. 10G, H) in two distinct growth phases that expanded northward from its initial ignition source (Fig. 10I). The small but fast burning White River fire, had a final burned extent of 16,164 burned ha (Fig. 10J, K) that grew southward from its initial ignition source in a mountainous region (Fig. 10L).

In addition, fire progressions can also be compared using the elapsed fire duration, from ignition to completion, to better compare fire-level behaviors and attributes (Fig. 11). The temporal window for days of fire was determined by the final day of growth to the final maximum fire size. For the Plateau fire, it was active for 122 days, with distinct burn periods throughout the active phase most notably on day 87 when relative burned area grew by 42% (Fig. 11A). The Plateau fire had a weekly observation rate of 1.72 observations per week during its actively burning period and 1.22 observations per week throughout the entire fire season. The Hanceville-Riske Creek fire had more dispersed burn periods throughout its 126-day actively burning period, with 23% relative growth on day 5 and 18% relative growth on day 101 (Fig. 11B). The Hanceville-Riske Creek fire had a weekly observation rate of 1.00 during its burning period and 1.5 throughout the entire fire season. The Elephant Hill fire had more steady burn periods without any distinct jumps of relative burned area growth $> 10\%$ throughout its 96-day burn period (Fig. 11C). The Elephant Hill fire had a weekly observation rate of 2.09 observations per week during its actively

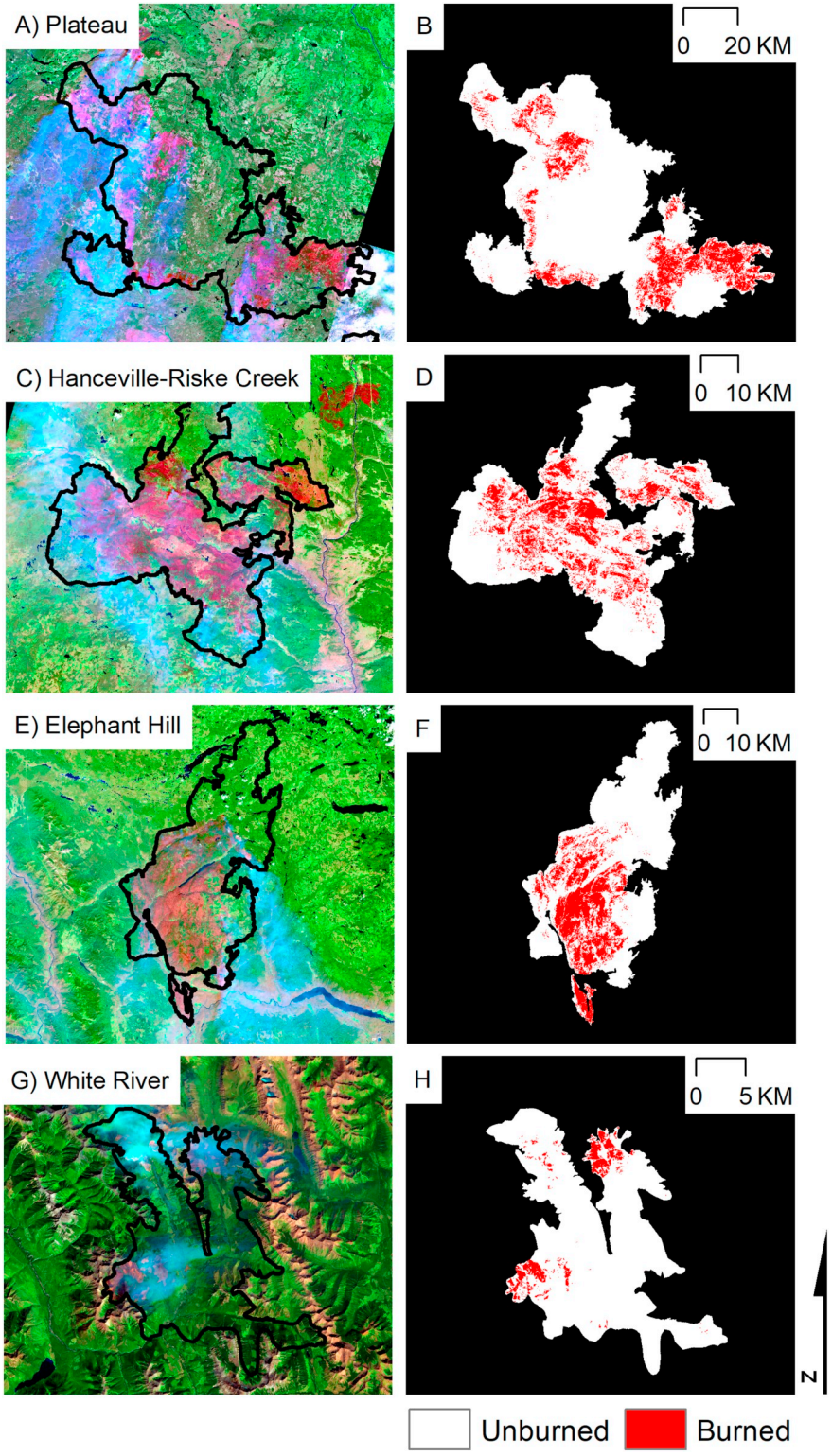

Fig. 9. For each fire (rows), intermediate burned area Landsat-8/Sentinel-2 composite in column 1 using the least-cloudy imagery from the nearest-in-time date from Landsat-8 or Sentinel-2 shown in Bands 7/12, 5/8, 3 (A, C, E, G) and intermediate BULC burned area dataset within the official CNFDB fire boundary zoomed on each fire in column 2 on September 2 (B), August 3 (D), August 4 (E), and September 1 (F).

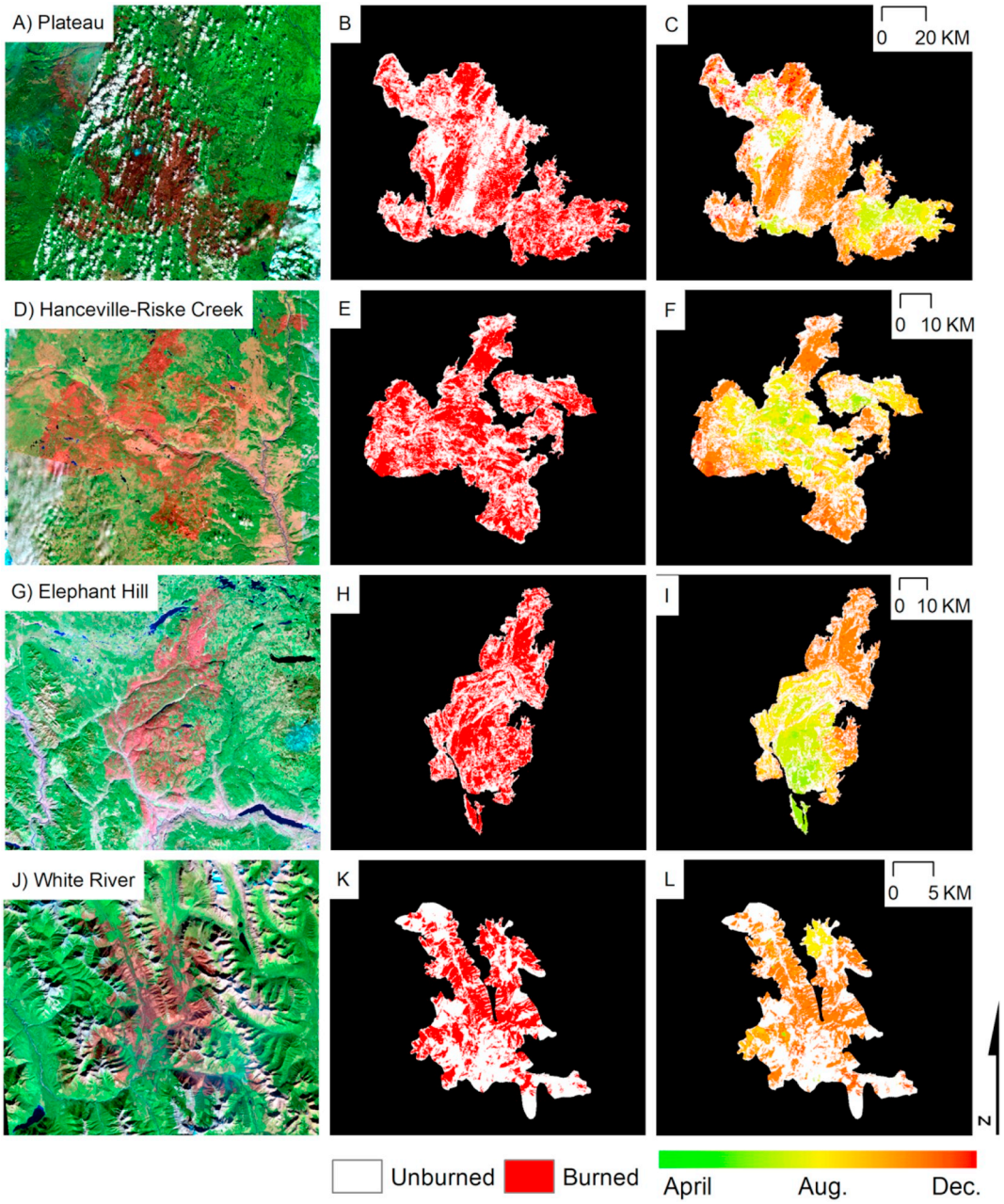

Fig. 10. For each fire (rows), final burned area Landsat-8/Sentinel-2 composite in column 1 for Bands 7,5,3/12,8,3 (A, D, G, J), final BULC burned area dataset within the official CNFDB fire boundary zoomed on each fire in column 2 (B, E, H, K), and fire-progression dataset shown from April to December in column 3 (C, E, I, L). In the Landsat-8 and Sentinel-2 composites in column 1, red areas correspond with burned area. The scale bar in column 3 is the same for all images in columns 1 and 2. (For interpretation of the references to colour in this figure legend, the reader is referred to the web version of this article.)

burning period and 1.22 observations per week throughout the entire fire season. The White River fire had very low burn periods until large spikes of relative growths of 23% on day 69 and 34% on day 71 in its 74-day actively burning periods (Fig. 11D). The White River fire had a weekly observation rate of 1.03 during its burning period and 2.27 throughout the entire fire season. The average relative weekly burn rate for each of the four fires throughout their actively burning weeks was between 8 and 11%. The 2017 fire season average for relative weekly burn rate was 26.6% with a range from 8.3% to 100%.

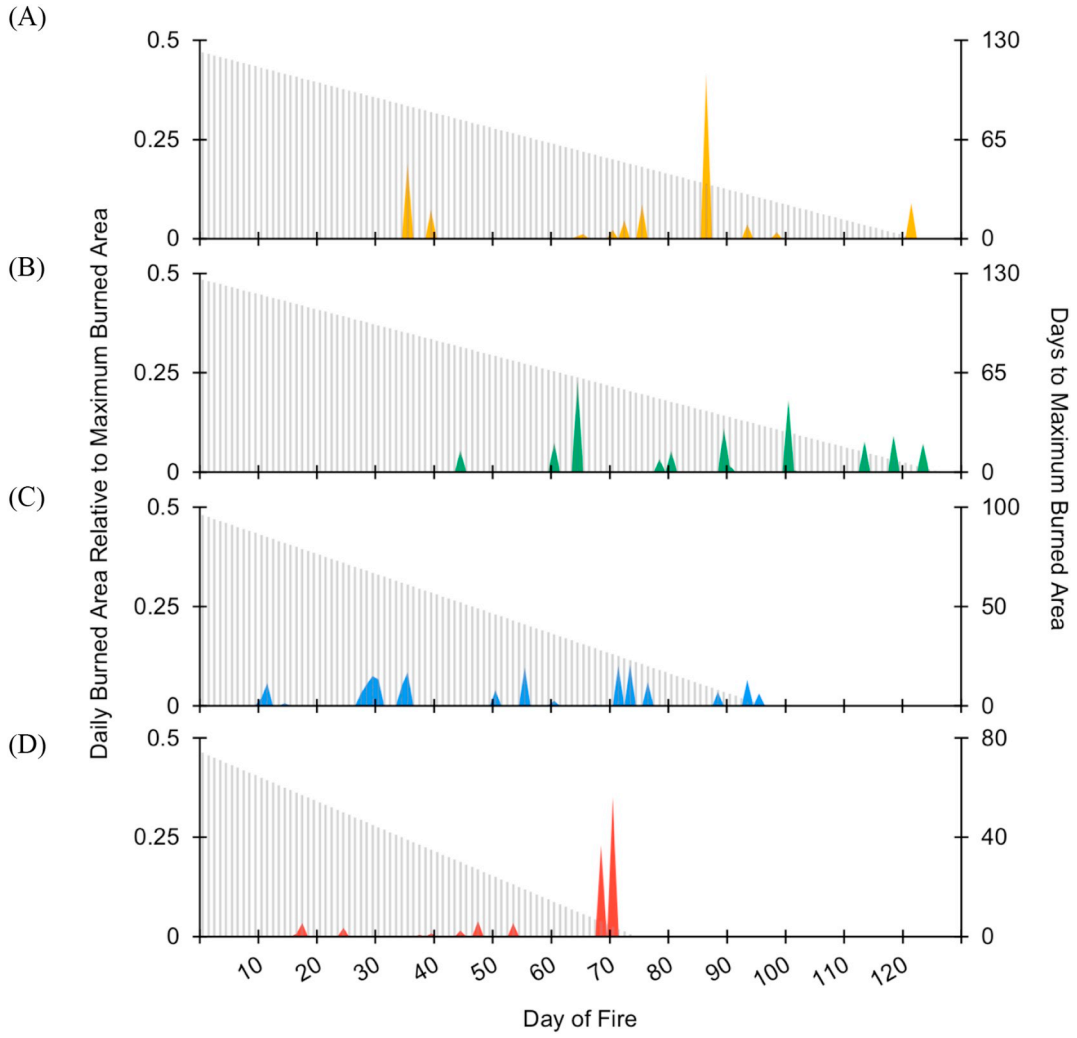

Fig. 11. Daily burned area relative to maximum burned areas for each of the (A) Plateau, (B) Hanceville-Riske Creek, (C) Elephant Hill, (D) White River fires, from normalized to days of fire rather than calendar date, with number of days until maximum burned date denoted in grey (secondary axis).

4. Discussion

Burned-area progression analyses were created for each of the 2017 fires in BC and created a large-area methodological approach for mapping the growth of fires throughout their active phases using data from multiple sources. Observation rate varied from fire to fire when creating this dataset over the extensive, BC-wide area for all 89 unique fires. The four largest fires from the study area shared characteristics as interface fires that were discovered in July. The largest and smallest fires presented, the Plateau and White River, both experienced two periods of large growth rates in August and September with fast burning characteristics. While both large fires, Elephant Hill and Hanceville-Riske Creek fires had more constant growth rates throughout their active phases. This work builds upon existing fire progression mapping methods outside of Canada that utilize the MO(Y)D14 active fire dataset to interpolate day-of-burn values for vectorized fire perimeters (e.g., Benali et al., 2016; Veraverbeke et al., 2014). The BULC approach advances fire progression methods by synthesizing fine-scale observations from multiple sensors to utilize the fine temporal resolution of coarse sensors like MODIS alongside the fine spatial scale resolution of sensors like Landsat and Sentinel-2. This enables weekly date-of-burn values derived for each pixel within the final fire perimeters at the spatial resolution of the input observations.

As presented in Figs. 3 and 4 the BULC product refines the burned/burning maps spatially compared with the existing datasets such as the CNFDB and NBAC burned-area dataset for mapping burned areas in British Columbia for the 2017 fire season. The spatial refinement of the BULC burned-area dataset relied heavily on Landsat and Sentinel-2 observations, which made up 94% of the total observations used as provisional classifications. Depending on the targeted use of burned-area datasets, the spatial scale and refinement necessary for analysis may vary. For example, the NBAC burned-area dataset provides burned area estimates that are more spatially generalized relative to the BULC fire-progression dataset, which may be preferable for providing less conservative estimates of carbon losses at the end of each season. However, if the burn-progression dataset is being used for targeting harvesting after the wildfires, then a more spatially-refined approach such as is provided by BULC may be preferred.

Near-real-time monitoring of disturbances is made possible through data-synthesis advancements for fusing observations from multiple sources (Li and Roy, 2017; Wulder et al., 2018). Although this approach does not currently provide real-time monitoring capacity, our long-term goal is to extend the approach to include a fire detection component by integrating active fire perimeters from provincial fire agencies. This would allow BULC to proceed mostly as described here, refining burned areas as new imagery arrived. By using active fire observations from multiple remote sensing sources, we were able to reduce the revisit interval provided by the sensors. BULC is a spectrally independent algorithm, which allows for the integration of data from multiple sources. In the case of mapping burned-area datasets, this allows for using the

most reliable burned-area classification protocol to classify imagery from varying sensors while also integrating information provided by previously-created burned-area datasets.

In a practical context, the highly automated approach to mapping provides a refined, spatially-explicit estimate of burned area that is available when the fire season concludes or at any time throughout the fire season. For all of BC fires, the burned-area estimate generated from this approach was within 16% of burned area estimates derived from a best-available composite mapping product that is typically generated retrospectively. The three largest fires have the greatest consequences for carbon loss and forest management and the burned-area estimates achieved with BULC were within 7.5% on average of NBAC burned-area estimates. Note that while correspondence to NBAC builds confidence in the generated BULC outputs, both products represent an estimate, and neither are truth. The approach demonstrated herein provides opportunities for actively mapping wildfires through the fire season to have running total of refined burned areas also highlighting locations of interest regarding carbon consequences and forest management and planning.

By increasing the number of data sources availed upon for mapping, such as using imagery from Landsat-7 in addition to Landsat-8, Sentinel-2, and MODIS, and by raising the cloud-cover threshold, we were able to retrospectively create fire observations at a sub-weekly scale. One challenge of using observations from cloudy, coarse, and scan line corrector-off (SLC-off; Wulder et al., 2011) imagery with no data is that there is a risk of causing temporal or spatial gaps in imaging. Temporal gaps occur when the fire grows, but there is a lack of clear observations to update the map. Additionally, spatial gaps arise when there are clear observations with partial-coverage that update portions of the fire. The benefit of using the observations from Landsat-7 is that its observations fill temporal gaps in the time series. The risk, however, is that its usage may propagate further spatial gaps and partial-image updates due to systematically missing data. For example, some of the Plateau Fire intermediary BULC-classifications contain strips of missing data in burned areas as the mapping relied largely on Landsat-7 imagery to provide temporal coverage. The benefit of including MODIS data is that its observations fill both temporal and spatial gaps in the time series. One trade-off is that production and release of the MODIS burned-area dataset takes approximately 4 months to deliver burned areas related to a given month. Another risk, however, is a coarsening of the final data product, whether in intermediary time steps or the dataset's duration. For example, a lack of data for several days for the Hanceville-Riske Creek and Elephant Hill fires caused anomalous spikes in burned-area estimations.

The impact of these temporal and spatial gaps in observations can be reduced in two ways; that is, using object-based knowledge to fill data gaps and increasing observations from non-optical sources. First, future methods can use segmentation to fill in spatial gaps within Landsat-7 provisional classifications (e.g., Wulder et al., 2004). Alternatively, BULC could update a series of pre-defined burned-area objects using evidence from partial observations to reduce spatial gaps. Second, there are opportunities to utilize observations from Synthetic-Aperture Radar (SAR) sensors such as Sentinel-1 to increase both temporal and spatial gaps from optical-sensor observations (Chuvieco et al., 2019). There are fewer algorithms for burned-area detection in Sentinel-1 imagery (e.g., Engelbrecht et al., 2017; Lohberger et al., 2018; Verhegghen et al., 2016), but even moderately reliable provisional classifications would provide gap-filling evidence for burned/burning pixels in the BULC algorithm.

The province-wide analysis opens new opportunities for understanding fire at regional, national, and continental scales. For example, comparisons can be made using this data source to relate characteristics of growing fires and act as validation for pre-existing forecasted fire weather datasets, fire behavior datasets, and existing wildland fire growth simulation models for Canada's boreal forest (Natural Resources Canada, 2018b; Fire Growth Model, 2018). Additional analyses can be performed to evaluate the relationship between underlying drivers of fire behavior (e.g., land cover, disturbance history) with the resulting fine-scale, patch-level fire progressions (e.g., Nogueira et al., 2016; Parks et al., 2018). Ultimately, the analysis area is not limited by the common constraints of disk space and processing speed because the provisional classification protocol and BULC algorithm are both programmed in Google Earth Engine. Information regarding fire progression through time, within a given year, offers insights regarding suppression success and enables linkages to potential drivers of fire spread.

5. Conclusion

In this study, we created and analyzed a fire-progression time series for all 89 fires in the historically large 2017 BC fire season using freely available data from multiple sensors and BULC. Working within the 2017 fire perimeters created by the BC Wildfire Service, we used over 1500 raw scenes from Landsat-7, Landsat-8, Sentinel-2 and MODIS to create 276 provisional input classifications. BULC was then used to merge the provisional classifications in Google Earth Engine, producing a synthesized time-series stack with updated weekly burned areas for the 2017 fire season for each fire in BC. This approach estimated burned areas for the 2017 fire season to within 16% of the estimates developed by the Canadian federal government in cooperation with provincial authorities for this fire season while uniquely also mapping fire progressions throughout the entire fire season.

By reconstructing fire progressions for actively burning fires using a multi-source satellite time series approach, we are able to examine burned-area attributes for the fire season and individual fires at varying temporal windows. Fires from the same fire season have varying attributes, whether small or large and quickly or slowly burning. A majority of the fires in the 2017 fire season were small and had rapid growth periods but accounted for $< 13\%$ of the cumulative fire area. Small and slow-growing fires accounted for only 3% of burned areas. Of the three largest fires investigated (e.g., Plateau, Hanceville-Riske, Elephant Hill), collectively representing 83% of the cumulative burned area for the 2017 fire season, burning was widespread but progressed at variable rates (both slow and rapid). Most of the behaviors and peak burn periods for the fire season were associated with weather events such as lightning and wind storms that occurred in early July and mid-September. Individual fires have varying burn progressions and different spatial patterns. By examining the daily burned areas of fires relative to total burned areas, we can quantify, compare, and contrast fire characteristics and the length of active burning phase.

This study reveals the potential for classifying multi-source, fire-progression stacks in other fire-prone regions and fire seasons utilizing our approach. Opportunities exist for increasing sources for fire observations for retrospective progression reconstruction and for implementing this approach for near-real-time fire monitoring to better inform fire agencies and forest managers. By implementing this approach using open-source satellite sources and remote sensing platforms, it can be applied on other historical fire seasons in Canada and tested for applicability internationally. Retrospective and near-term fire-classification stacks like these for historical and future fire seasons can be used to analyze underlying fire ecology and inform future disaster management.

Acknowledgements

Open Access supported by the Government of Canada. This research was undertaken as part of the ‘Earth Observation to Inform Canada's Climate Change Agenda (EO3C)’ project jointly funded by the Canadian Space Agency (CSA), Government Related Initiatives Program (GRIP), and the Canadian Forest Service (CFS) of Natural Resources Canada. This research was enabled in part by support provided by WestGrid

(www.westgrid.ca) and Compute Canada (www.computecanada.ca). Many thanks to Nicolas Rivarola, Sara Pancheri, and Eric Davies. This manuscript benefitted from the insights of three anonymous reviewers.

References

Abatzoglou, J.T., Williams, A.P., 2016. Impact of anthropogenic climate change on wildfire across western US forests. Proc. Natl. Acad. Sci. 113 (42), 11770–11775.

Abbott, G., Chapman, M., 2018. Addressing the New Normal: 21st Century Disaster Management in British Columbia. British Columbia Government Report. pp. 1–140. https://www2.gov.bc.ca/assets/gov/public-safety-and-emergency-services/emergency-preparedness-response-recovery/embc/bc-flood-and-wildfire-review-addressing-the-new-normal-21st-century-disaster-management-in-bc-web.pdf.

Achanta, R., Süsstrunk, S., 2017. Superpixels and polygons using simple non-iterative clustering. In: 2017 IEEE Conference Computer Vision and Pattern Recognition (CVPR), pp. 4895–4904.

Amiro, B.D., Todd, J.B., Wotton, B.M., Logan, K.A., Flannigan, M.D., Stocks, B.J., Mason, J.A., Martell, D.L., Hirsch, K.G., 2001. Direct carbon emissions from Canadian forest fires, 1959–1999. Can. J. For. Res. 31 (3), 512–525.

BC Wildfire Service, 2017a. Wildfire season summary. https://www2.gov.bc.ca/gov/content/safety/wildfire-status/about-bcws/wildfire-history/wildfire-season-summary, Accessed date: 28 October 2018.

BC Wildfire Service, 2017b. PROT_CURRENT_FIRE_POLYS_SP Ministry of Forests, Lands, Natural Resource Operations and Rural Development. https://catalogue.data.gov.bc.ca/dataset/fire-perimeters-current, Accessed date: 25 January 2018.

BC Wildfire Service, 2017c. Wildfires of Note - Plateau Fire (C0784). http://bcfireinfo.for.gov.bc.ca/hprScripts/WildfireNews/OneFire.asp?ID=645, Accessed date: 28 October 2018.

BC Wildfire Service, 2017d. Wildfires of Note – Hanceville-Riske Creek (C50647). http://bcfireinfo.for.gov.bc.ca/hprScripts/WildfireNews/OneFire.asp?ID=666, Accessed date: 28 October 2018.

BC Wildfire Service, 2017e. Wildfires of Note - Elephant Hill (K20637). http://bcfireinfo.for.gov.bc.ca/hprScripts/WildfireNews/OneFire.asp?ID=620, Accessed date: 28 October 2018.

BC Wildfire Service, 2017f. Wildfires of Note – White River Fire (N1628). http://bcfireinfo.for.gov.bc.ca/hprScripts/WildfireNews/OneFire.asp?ID=678, Accessed date: 28 October 2018.

Benali, A., Russo, A., Sá, A.C., Pinto, R., Price, O., Koutsias, N., Pereira, J., 2016. Determining fire dates and locating ignition points with satellite data. Remote Sens. 8 (4), 326.

Blaschke, T., 2010. Object based image analysis for remote sensing. ISPRS J. Photogramm. Remote Sens. 65 (1), 2–16.

Boschetti, L., Roy, D.P., Justice, C.O., Humber, M.L., 2015. MODIS–Landsat fusion for large area 30m burned area mapping. Remote Sens. Environ. 161, 27–42.

Bowman, D., 2018. Wildfire science is at a loss for comprehensive data. Nature 560 (7). https://doi.org/10.1038/d41586-018-05840-4.

British Columbia, 2018. Remembering 2017: looking back a year later at the start of the 2017 wildfire season for the Cariboo Fire Centre. https://www2.gov.bc.ca/gov/content/safety/wildfire-status/about-bcws/wildfire-history/remembering-2017, Accessed date: 28 October 2018.

Burton, P.J., Parisien, M.A., Hicke, J.A., Hall, R.J., Freeburn, J.T., 2009. Large fires as agents of ecological diversity in the North American boreal forest. Int. J. Wildland Fire 17 (6), 754–767.

Canadian Council of Forest Ministers, 2018. Forest Fires. http://nfdp.ccfm.org/en/data/fires.php, Accessed date: 30 October 2018.

Cardille, J.A., Fortin, J.A., 2016. Bayesian updating of land-cover estimates in a data-rich environment. Remote Sens. Environ. 186, 234–249.

Chuvieco, E., Mouillot, F., van der Werf, G.R., San Miguel, J., Tanasse, M., Koutsias, N., García, M., Yebra, M., Padilla, M., Gitas, I., Heil, A., 2019. Historical background and current developments for mapping burned area from satellite earth observation. Remote Sens. Environ. 225, 45–64.

Crowley, M.A., Cardille, J.A., White, J.C., Wulder, M.A., 2019. Multi-sensor, multi-scale, Bayesian data synthesis for mapping within-year wildfire progression. Remote Sens. Lett 10 (3), 302–311. https://doi.org/10.1080/2150704X.2018.1536300. 2019.

de Groot, W.J., Landry, R., Kurz, W.A., Anderson, K.R., Englefield, P., Fraser, R.H., Hall, R.J., Banfield, E., Raymond, D.A., Decker, V., Lynham, T.J., 2007. Estimating direct carbon emissions from Canadian wildland fires. Int. J. Wildland Fire 16 (5), 593–606. https://doi.org/10.1071/WF06150.

de Groot, W.J., Pritchard, J.M., Lynham, T.J., 2009. Forest floor fuel consumption and carbon emissions in Canadian boreal forest fires. Can. J. For. Res. 39 (2), 367–382. https://doi.org/10.1139/X08-192.

Egorov, A.V., Roy, D.P., Zhang, H.K., Hansen, M.C., Kommareddy, A., 2018. Demonstration of percent tree cover mapping using Landsat Analysis Ready Data (ARD) and sensitivity with respect to Landsat ARD processing level. Remote Sens. 10 (2), 209.

Engelbrecht, J., Theron, A., Vhengani, L., Kemp, J., 2017. A simple normalized difference approach to burnt area mapping using multi-polarisation C-band SAR. Remote Sens. 9 (8), 764.

Fire Growth Model, 2018. Prometheus - Overview. http://www.firegrowthmodel.ca/prometheus/overview_e.php, Accessed date: 28 October 2018.

Fraser, R.H., Li, Z., Cihlar, J., 2000. Hotspot and NDVI differencing synergy (HANDS): a new technique for burned area mapping over boreal forest. Remote Sens. Environ. 74 (3), 362–376.

Fraser, R.H., Hall, R.J., Landry, R., Lynham, T., Raymond, D., Lee, B., Li, Z., 2004. Validation and calibration of Canada-wide coarse-resolution satellite burned-area maps. Photogramm. Eng. Remote. Sens. 70 (4), 451–460.

Frazier, R.J., Coops, N.C., Wulder, M.A., Hermosilla, T., White, J.C., 2018. Analyzing spatial and temporal variability in short-term rates of post-fire vegetation return from Landsat time series. Remote Sens. Environ. 205, 32–45.

Giglio, L., Justice, C., Boschetti, L., Roy, D., 2015. MCD64A1 MODIS/Terra + Aqua Burned Area Monthly L3 Global 500m SIN Grid V006. NASA EOSDIS Land Processes DAAC. https://doi.org/10.5067/MODIS/MCD64A1.006, Accessed date: 1 March 2018.

Gitas, I.Z., Mitri, G.H., Ventura, G., 2004. Object-based image classification for burned area mapping of Creus Cape, Spain, using NOAA-AVHRR imagery. Remote Sens. Environ. 92 (3), 409–413.

Gorelick, N., Hancher, M., Dixon, M., Ilyushchenko, S., Thau, D., Moore, R., 2017. Google earth engine: planetary-scale geospatial analysis for everyone. Remote Sens. Environ. 202, 18–27.

Hall, R.J., Freeburn, J.T., De Groot, W.J., Pritchard, J.M., Lynham, T.J., Landry, R., 2008. Remote sensing of burn severity: experience from western Canada boreal fires. Int. J. Wildland Fire 17 (4), 476–489.

Hermosilla, T., Wulder, M.A., White, J.C., Coops, N.C., Hobart, G.W., Campbell, L.B., 2016. Mass data processing of time series Landsat imagery: pixels to data products for forest monitoring. Int. J. Digital Earth 9 (11), 1035–1054.

Hermosilla, T., Wulder, M.A., White, J.C., Coops, N.C., Hobart, G.W., 2017. Updating Landsat time series of surface-reflectance composites and forest change products with new observations. Int. J. Appl. Earth Obs. Geoinf. 63, 104–111.

Hilker, T., Wulder, M.A., Coops, N.C., Linke, J., McDermid, G., Masek, J.G., Gao, F., White, J.C., 2009a. A new data fusion model for high spatial-and temporal-resolution mapping of forest disturbance based on Landsat and MODIS. Remote Sens. Environ. 113 (8), 1613–1627.

Hilker, T., Wulder, M.A., Coops, N.C., Seitz, N., White, J.C., Gao, F., Masek, J.G., Stenhouse, G., 2009b. Generation of dense time series synthetic Landsat data through data blending with MODIS using a spatial and temporal adaptive reflectance fusion model. Remote Sens. Environ. 113 (9), 1988–1999.

Humber, M.L., Boschetti, L., Giglio, L., Justice, C.O., 2018. Spatial and temporal inter-comparison of four global burned area products. Int. J. Digital Earth 1–25.

Jolly, W.M., Cochrane, M.A., Freeborn, P.H., Holden, Z.A., Brown, T.J., Williamson, G.J., Bowman, D.M., 2015. Climate-induced variations in global wildfire danger from 1979 to 2013. Nat. Commun. 6, 7537.

Key, C.H., Benson, N.C., 1999. Measuring and remote sensing of burn severity. In: Neuenschwander, L.F., Ryan, K.C. (Eds.), Proceedings Joint Fire Science Conference and Workshop. II. University of Idaho and International Association of Wildland Fire, Moscow, ID, pp. 284.

Key, C.H., Benson, N.C., 2006. Landscape assessment (LA). FIREMON: Fire effects monitoring and inventory system. In: Lutes, D.C., Keane, R.E., Carati, J.F., Key, C.H., Benson, N.C., Gangi, L.J. (Eds.), General Technical Report RMRS-GTR-164-CD (Pp. LA−1-55). USDA Forest Service, Rocky Mountains Research Station, Fort Collins, CO. https://doi.org/10.2737/RMRS-GTR-164.

Korhonen, L., Hadi, Packalen, P., Rautiainen, M., 2017. Comparison of Sentinel-2 and Landsat 8 in the estimation of boreal forest canopy cover and leaf area index. Remote Sens. Environ. 195, 259–274.

Lee, J., Cardille, J., Coe, M., 2018. BULC-U: sharpening resolution and improving accuracy of land-use/land-cover classifications in Google Earth Engine. Remote Sens. 10 (9), 1455.

Li, J., Roy, D.P., 2017. A global analysis of sentinel-2A, sentinel-2B and Landsat-8 data revisit intervals and implications for terrestrial monitoring. Remote Sens. 9 (9), 902.

Lohberger, S., Stängel, M., Atwood, E.C., Siegert, F., 2018. Spatial evaluation of Indonesia's 2015 fire-affected area and estimated carbon emissions using Sentinel-1. Glob. Chang. Biol. 24 (2), 644–654.

Mora, B., Wulder, M.A., White, J.C., Hobart, G., 2013. Modeling stand height, volume, and biomass from very high spatial resolution satellite imagery and samples of airborne LiDAR. Remote Sens. 5 (5), 2308–2326.

Natural Resources Canada, 2018a. nbac_2017_r2_20180725_1603.Zip Canadian National Fire Database - National Burned Area Composite. http://cwfis.cfs.nrcan.gc.ca/downloads/nbac/, Accessed date: 10 September 2018.

Natural Resources Canada, 2018b. Monthly and Seasonal Forecasts - Canadian Wildland Fire Information System. http://cwfis.cfs.nrcan.gc.ca/maps/forecasts, Accessed date: 28 October 2018.

Nogueira, J.M., Ruffault, J., Chuvieco, E., Mouillot, F., 2016. Can we go beyond burned area in the assessment of global remote sensing products with fire patch metrics? Remote Sens. 9 (1), 7.

Padilla, M., Stehman, S.V., Chuvieco, E., 2014. Validation of the 2008 MODIS-MCD45 global burned area product using stratified random sampling. Remote Sens. Environ. 144, 187–196.

Padilla, M., Stehman, S.V., Ramo, R., Corti, D., Hantson, S., Oliva, P., Alonso-Canas, I., Bradley, A.V., Tansey, K., Mota, B., Pereira, J.M., 2015. Comparing the accuracies of remote sensing global burned area products using stratified random sampling and estimation. Remote Sens. Environ. 160, 114–121.

Parisien, M.A., Peters, V.S., Wang, Y., Little, J.M., Bosch, E.M., Stocks, B.J., 2006. Spatial patterns of forest fires in Canada, 1980–1999. Int. J. Wildland Fire 15 (3), 361–374.

Parisien, M.A., Parks, S.A., Miller, C., Krawchuk, M.A., Heathcott, M., Moritz, M.A., 2011. Contributions of ignitions, fuels, and weather to the spatial patterns of burn probability of a boreal landscape. Ecosystems 14 (7), 1141–1155. https://doi.org/10.1007/S10021-011-9474-2.

Parks, S.A., 2014. Mapping day-of-burning with coarse-resolution satellite fire-detection data. Int. J. Wildland Fire 23 (2), 215–223.

Parks, S.A., Parisien, M.A., Miller, C., 2012. Spatial bottom-up controls on fire likelihood vary across western North America. Ecosphere 3 (1), 1–20. https://doi.org/10.1890/

ES11-00298.1.
Parks, S.A., Holsinger, L.M., Panunto, M.H., Jolly, W.M., Dobrowski, S.Z., Dillon, G.K., 2018. High-severity fire: evaluating its key drivers and mapping its probability across western US forests. Environ. Res. Lett. 13 (4), 044037.
Quintano, C., Fernández-Manso, A., Fernández-Manso, O., 2018. Combination of Landsat and Sentinel-2 MSI data for initial assessing of burn severity. Int. J. Appl. Earth Obs. Geoinf. 64, 221–225.
Roy, D.P., Wulder, M.A., Loveland, T.R., Woodcock, C.E., Allen, R.G., Anderson, M.C., Helder, D., Irons, J.R., Johnson, D.M., Kennedy, R., Scambos, T.A., 2014. Landsat-8: science and product vision for terrestrial global change research. Remote Sens. Environ. 145, 154–172.
San-Miguel, I., Andison, D.W., Coops, N.C., 2017. Characterizing historical fire patterns as a guide for harvesting planning using landscape metrics derived from long term satellite imagery. For. Ecol. Manag. 399, 155–165. https://doi.org/10.1016/j.foreco.2017.05.021.
San-Miguel, I., Andison, D.W., Coops, N.C., 2018. Quantifying local fire regimes using the Landsat data-archive: a conceptual framework to derive detailed fire pattern metrics from pixel-level information. Int. J. Digital Earth 1–22. https://doi.org/10.1080/17538947.2018.1464072.
Schroeder, T.A., Wulder, M.A., Healey, S.P., Moisen, G.G., 2011. Mapping wildfire and clearcut harvest disturbances in boreal forests with Landsat time series data. Remote Sens. Environ. 115 (6), 1421–1433.
Soverel, N.O., Perrakis, D.D., Coops, N.C., 2010. Estimating burn severity from Landsat dNBR and RdNBR indices across western Canada. Remote Sens. Environ. 114 (9), 1896–1909.
Soverel, N.O., Coops, N.C., Perrakis, D.D., Daniels, L.D., Gergel, S.E., 2011. The transferability of a dNBR-derived model to predict burn severity across 10 wildland fires in western Canada. Int. J. Wildland Fire 20 (4), 518–531.
Stinson, G., Kurz, W.A., Smyth, C.E., Neilson, E.T., Dymond, C.C., Metsaranta, J.M., Boisvenue, C., Rampley, G.J., Li, Q., White, T.M., Blain, D., 2011. An inventory-based analysis of Canada's managed forest carbon dynamics, 1990 to 2008. Glob. Chang. Biol. 17 (6), 2227–2244.
Stocks, B.J., Mason, J.A., Todd, J.B., Bosch, E.M., Wotton, B.M., Amiro, B.D., Flannigan, M.D., Hirsch, K.G., Logan, K.A., Martell, D.L., Skinner, W.R., 2003. Large forest fires in Canada, 1959–1997. J. Geophys. Res. Atmos. 108, 1–12. https://doi.org/10.1029/2001.JD000484. (D1: FFR5).
U. S. Geological Survey, 2018. U.S. Landsat Analysis Ready Data (ARD) Data Format Control Book (DFCB). LSDS-809. US Department of Interior, Earth Resources Observation and Science (EROS) Center, Sioux Falls, SD. https://landsat.usgs.gov/sites/default/files/documents/LSDS-1873_US_Landsat_ARD_DFCB.pdf, Accessed date: 15 April 2018.
Veraverbeke, S., Somers, B., Gitas, I., Katagis, T., Polychronaki, A., Goossens, R., 2012. Spectral mixture analysis to assess post-fire vegetation regeneration using Landsat thematic mapper imagery: accounting for soil brightness variation. Int. J. Appl. Earth Obs. Geoinf. 14 (1), 1–11.
Veraverbeke, S., Sedano, F., Hook, S.J., Randerson, J.T., Jin, Y., Rogers, B.M., 2014. Mapping the daily progression of large wildland fires using MODIS active fire data. Int. J. Wildland Fire 23 (5), 655–667.
Verhegghen, A., Eva, H., Ceccherini, G., Achard, F., Gond, V., Gourlet-Fleury, S., Cerutti, P., 2016. The potential of Sentinel satellites for burnt area mapping and monitoring in the Congo Basin forests. Remote Sens. 8 (12), 986.
White, J.C., Wulder, M.A., Hobart, G.W., Luther, J.E., Hermosilla, T., Griffiths, P., Coops, N.C., Hall, R.J., Hostert, P., Dyk, A., Guindon, L., 2014. Pixel-based image compositing for large-area dense time series applications and science. Can. J. Remote. Sens. 40 (3), 192–212.
White, J.C., Wulder, M.A., Hermosilla, T., Coops, N.C., Hobart, G.W., 2017. A nationwide annual characterization of 25 years of forest disturbance and recovery for Canada using Landsat time series. Remote Sens. Environ. 194, 303–321.
Wulder, M.A., Skakun, R.S., Kurz, W.A., White, J.C., 2004. Estimating time since forest harvest using segmented Landsat ETM+ imagery. Remote Sens. Environ. 93 (1–2), 179–187.
Wulder, M.A., White, J.C., Gillis, M.D., Walsworth, N., Hansen, M.C., Potapov, P., 2010. Multiscale satellite and spatial information and analysis framework in support of a large-area forest monitoring and inventory update. Environ. Monit. Assess. 170 (1–4), 417–433.
Wulder, M.A., White, J.C., Masek, J.G., Dwyer, J., Roy, D.P., 2011. Continuity of Landsat observations: short term considerations. Remote Sens. Environ. 115 (2), 747–751.
Wulder, M.A., Coops, N.C., Roy, D.P., White, J.C., Hermosilla, T., 2018. Land cover 2.0. Int. J. Remote Sens. 39 (12), 4254–4284. https://doi.org/10.1080/01431161.2018.1452075.
Zhu, Z., 2017. Change detection using Landsat time series: a review of frequencies, preprocessing, algorithms, and applications. ISPRS J. Photogramm. Remote Sens. 130, 370–384.